

Magnetic Properties of GeNi_2O_4 Under High Pressure and Magnetic Dilution

J.T. Korobanik,^{1,*} K. Caslin,^{1,2} P. Reuvekamp,² and F.S. Razavi¹

¹*Dept. of Physics, Brock University, 500 Glenridge Ave, St Catharines, ON, L2S 3A1, Canada*

²*Max-Planck-Institute for Solid State Research, Heisenbergstrasse 1, D-70569 Stuttgart, Germany*

(Dated: August 30, 2018)

The effects of magnetic dilution and applied pressure on frustrated spinel $\text{Ni}_{2-x}\text{Mg}_x\text{GeO}_4$ ($0 \leq x \leq 1.0$) are analyzed using specific heat, AC and DC magnetization and x-ray diffraction. The parent compound has two closely spaced antiferromagnetic transitions $T_{\text{N}1} = 12.0$ K (kagomé planes) and $T_{\text{N}2} = 11.4$ K (triangular planes). In the dilution range tested the low temperature magnetic state takes three forms: antiferromagnetic ($0 \leq x \leq 0.05$), ill-defined ($x = 0.10$ and 0.15), and spin glass ($0.30 \leq x \leq 1.0$). The AFM region shows an extreme vulnerability to dilution with a percolation threshold of $p_{c1} = 0.74 \pm 0.04$ and $p_{c2} = 0.65 \pm 0.05$ for the kagomé and triangular planes respectively, which are much larger than expected for 3D systems. We suggest that this behavior is due to coupling between the kagomé and triangular spins forming a 'network of networks' (NON). Thermal expansion data on parent NGO indicates a field dependent lattice contraction during ordering events. Furthermore, there is a transition from contraction to expansion in an applied field of 6 T in the kagomé planes. For dilution levels $x \geq 0.30$, the system becomes a spin glass with canonical behavior. Specific heat results suggest that the triangular spins become disordered with increasing Mg^{2+} substitution followed by the onset of glassiness in the kagomé planes. Furthermore, there appears to be a dilution driven shift from 3 dimensional to 2 dimensional behavior as the low temperature magnetic heat capacity scales as T^2 in the spin glass state.

PACS numbers: 75.50.Lk, 75.30.Kz, 75.40.-s

I. INTRODUCTION

Geometrically frustrated materials have garnered much research attention due to the multitude of complex low temperature states they exhibit.¹⁻⁵ Magnetic analogues of structurally disordered systems such as spin ice⁶ and spin glass⁷ have been extensively studied.⁸ The essence of magnetic frustration is the inability to simultaneously satisfy magnetic interactions. When this arises from the physical layout of magnetic ions, it is termed geometric frustration.⁹ This competition between magnetic interactions can preclude the formation of a distinct magnetic ground state.¹⁰ The low temperature state is often determined by small perturbations such as dipole-dipole interactions, structural changes and impurities which act to lift the degeneracy and relieve frustration.¹¹ Typically, this results in a T_c at lower temperatures due to the effective quenching of exchange. Geometric frustration often occurs in triangular based structures under antiferromagnetic (AFM) nearest neighbor exchange. Examples of these are edge-sharing triangular and corner-sharing triangular (kagomé) lattices. Three dimensional realizations of these often occur in materials with pyrochlore and spinel structures.¹²

GeNi_2O_4 (NGO) crystallizes in olivine or spinel structure types depending on growth conditions.¹³ Materials that crystallize with spinel structure (AB_2O_4) are composed of B sites with octahedral coordination and A sites with tetrahedral coordination. One can view this structure as two inter-penetrating diamond and pyrochlore sub-lattices that are associated with either the A-site (diamond) or B-site (pyrochlore). When viewing the B sub-lattice along the $[111]$ direction, one observes al-

ternate stacking of kagomé and triangular planes which is highlighted in Fig. 1. Geometric magnetic frustration can result from an AFM exchange between B site ions ($\text{B}=\text{Mn}^{3+}$, Cr^{3+} , V^{3+} , Fe^{3+}).¹⁴ The parameter¹⁰ $f = |\theta_{\text{cw}}|/T_c$, which is a measure of Néel suppression, is often used to characterize the strength of frustration. For example, the spinel ZnCr_2O_4 has a very high value $f=31.2$ and has been shown to order after a lattice distortion from cubic to tetragonal.¹⁵ Neutron diffraction studies have indicated the formation of a complex coplanar spin state at low temperature.³ Regarding Germanates, several compounds form with spinel structures such as GeCo_2O_4 ¹⁶ and, under high pressure conditions, GeCu_2O_4 ¹⁷.

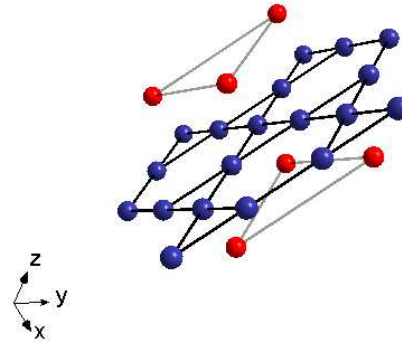


FIG. 1. [color online] Simplified illustration of B-site sublattice in GeNi_2O_4 spinel. All spheres are Ni^{2+} ions with blue representing those in kagomé layers and red representing those in triangular layers.

Interest in GeNi_2O_4 has grown due to the existence of two closely spaced magnetic transitions at $T_{\text{N}1} = 12.0$ K and $T_{\text{N}2} = 11.4$ K.¹⁸ Neutron diffraction studies¹⁹ on single crystals indicate that these ordering phenomena are due to the alignment of spins within the stacked kagomé and triangular planes. Specifically, at $T_{\text{N}1}$ the spins within the kagomé planes align ferromagnetically with AFM alignment between successive like-planes. At $T_{\text{N}2}$ the triangular planes arrange themselves in the same fashion. To describe this ordering behaviour a large exchange network with a dominant fourth nearest-neighbour J_4 term is required.¹⁹ The degeneracy of 3d orbitals for Ni^{2+} ions (3F_4) in octahedral crystal field is lifted with a ground state of $S=1$. The triplet t_{2g} levels are further split by spin-orbit coupling but this contribution is very small and can be ignored.^{16,20} Specific heat data have shown that only approximately 60% of the expected magnetic entropy is recovered. In addition, the entropy change associated with each ordering event is nearly the same which is unusual as three times as many spins reside on the kagomé compared to the triangular planes.

Magnetic dilution is an important technique in determining information on the several parameters about the exchange interactions in magnetically ordered systems. Replacing magnetic ions with non-magnetic analogues removes sites that can participate in magnetic exchange. This has a destabilizing effect on long range order (LRO) which reduces ordering temperature in a fashion dictated by the dimensionality and length scale of the interactions. When dealing with frustrated systems, dilution often produces a spin glass which is a disordered meta-stable state which forms below a well defined freezing temperature T_f . In Ga^{3+} diluted Zinc Chromate $\text{ZnCr}_{2-x}\text{Ga}_x\text{O}_4$, the AFM state gives way to a spin glass at $x = 0.2^{21}$ ($x = 0.4^{22}$ for bulk magnetic probes).

This work focuses on the effects of magnetic dilution and applied pressure on the ordering behaviour of GeNi_2O_4 . Specifically, on the magnetic and physical properties of polycrystalline samples of $\text{GeNi}_{2-x}\text{Mg}_x\text{O}_4$ ($x = 0$ to 1.0). The phase diagram of this family of compounds is determined using bulk probes. Particularly, we seek to understand how these contributions will effect each transition, as they are linked to particular planes (kagomé or triangular). Results contain herein indicate $\text{GeNi}_{2-x}\text{Mg}_x\text{O}_4$ exists in three distinct magnetic phases: antiferromagnetic ($0 \leq x \leq 0.05$), ill-defined ($x=0.10$ and 0.15), and spin glass ($x \geq 0.30$). The ordered kagomé and triangular planes, associated with the AFM state, are extremely vulnerable to magnetic dilution as indicated by large percolation thresholds. We suggest that these anomalous values can be explained by a coupled network effect which causes early failure in the LRO state. This weakness to dilution is contrasted by how robust $T_{\text{N}1}$ and $T_{\text{N}2}$ are to applied pressure. In the spin glass regime, T^2 dependence of the magnetic specific heat reveals a 3D to 2D shift in the behavior of the system due to dilution.

II. EXPERIMENTAL

Polycrystalline samples of $\text{GeNi}_{2-x}\text{Mg}_x\text{O}_4$ ($x = 0, 0.01, 0.02, 0.03, 0.04, 0.05, 0.10, 0.15, 0.30, 0.45, 0.60, 0.80, 1.0$) were formed using solid state synthesis. High purity powders of NiO, MgO and GeO_2 were mixed and wet milled in acetone. The mixture was placed in an alumina crucible and fired 1373 K for 12 hours. This was repeated, followed by pellet formation, and a heat treatment of 1473 K for 4 hours. The resulting compound was a light green color which became lighter for diluted samples.

DC susceptibility measurements were taken using a Quantum Design Magnetic Property Measurement System (MPMS). Specific heat and AC susceptibility data were obtained using a Quantum Design Physical Property Measurement System (PPMS).

High pressure measurements were taken using a custom built pressure cell which is capable of reaching 1.2 GPa. Degassed glycerine was used as a pressure medium and a small piece high purity lead (99.999%) as a manometer. Internal cell pressure was determined by measuring the superconducting transition of the lead,²³ which was placed in a teflon capsule along with the sample and pressure medium.

III. RESULTS

A. X Ray Diffraction

X ray powder diffraction data was refined to determine phase formation and lattice constants. No impurity phase or starting material Bragg peaks were observed. Refinement data is found in Table I. There is an observed expansion of lattice parameter with increased dilution that does not appear to be linear in nature. An expansion of lattice parameter for the substitution of Mg with Ni is expected as the crystal radii of Mg and Ni are 0.71 Å and 0.63 Å respectively.²⁴ However, the non-linear response has been theoretically predicted in systems with $\alpha = 0.88$ where α is the ratio of ionic radii ($\alpha = 0.89$ for Mg^{2+} and Ni^{2+} in octahedral environments).²⁵ At dilution levels of approximately 55%, the material crystallizes in both olivine and spinel forms, with full Mg^{2+} substitution in the spinel structure occurring when high pressure synthesis techniques are used.¹³

B. DC Susceptibility

DC susceptibility data have been reported in literature for GeNi_2O_4 , but inconsistencies exist between authors. For example, ordering temperatures $T_{\text{N}1}$ and $T_{\text{N}2}$ of 11.4K and 12.0K are agreed upon; however, various Currie-Weiss (CW) temperature Θ_{cw} values such as -15 K²⁶, -8.7 K¹⁶, -4.4 K¹⁸ are reported. Our measurements of GeNi_2O_4 successfully reproduced the CW re-

TABLE I. Summary of data on samples of parent and diluted NGO. Dilution (%) is Mg concentration, superscripts indicate n (Néel), f (spin glass), + (ill defined) transitions. Results from Rietveld refinement are given as lattice constant a and the corresponding χ^2 .

Dilution (%)	$T_{n,f}$ (K)	θ_{CW} (K)	a (Å)	χ^2
0	ⁿ 11.41, ⁿ 12.01	15.0 ± 0.5	8.218(1)	1.25
2.5	ⁿ 10.89	14.8 ± 0.2	8.219(0)	1.36
5.0	⁺ 9.0	15.1 ± 0.2	8.219(0)	1.6
7.5	⁺ 7.76	13.5 ± 0.3	8.220(1)	1.74
15	^f 7.41	9.4 ± 0.3	8.221(7)	1.27
22.5	^f 7.03	9.2 ± 0.3	8.221(5)	1.3
30	^f 6.75	9.1 ± 0.2	8.221(7)	1.35
40	^f 6.14	7.52 ± 0.09	8.222(8)	1.22
50	^f 5.35	6.40 ± 0.07	8.227(4)	1.20

sults obtained by Diaz *et al* through the addition of a diamagnetic term $\chi_{\text{dia}} = 7.20 \times 10^{-5}$ emu/mol_{NGO} and a temperature independent paramagnetic (TIP) term $\chi_{\text{ind}} = 7.42 \times 10^{-4}$ emu/mol_{NGO}. This TIP value is reasonable for Ni^{2+} in an octahedral crystal field with a splitting of 8000 cm^{-1} .²⁷

$$\chi_{\text{ind}} \propto \frac{4}{\Delta} \quad (1)$$

where Δ is the wavenumber splitting to the first excited state, which is large enough to not be thermally populated. These contributions were scaled appropriately for all of the diluted samples.

Results from DC magnetic data analysis are given in Table I. One can identify two regions ($0.15 \leq x \leq 0.6$ and $0.60 \leq x \leq 1.0$) of linear behavior in θ_{CW} with respect to dilution. Extrapolating a linear fit line to full dilution yields $\theta_{CW}=0$ within associated error. A similar kink in $\theta_{CW}(p)$ has been observed in other diluted frustrated systems, such as $\text{SrGa}_{12-x}\text{Cr}_x\text{O}_{19}$ (SGCO(x)).²⁸

In spin glasses, when the system is cooled below the freezing temperature, it freezes in a metastable state. This instability can be probed using thermoremanent magnetization (M_{TRM}), which measures the decay of the magnetic susceptibility with time. Our cooling and field routine consists of applying a 2000 Oe field at 300 K. The system is cooled to 2 K over 12000 seconds. The field is then turned off following a wait time of 600 seconds. Once the applied field is removed, the magnetization is measured for 10000 seconds.

$$M_{TRM} = M_0 e^{-(\frac{t}{\tau})^{1-n}} \quad (2)$$

The decay of the resulting moment for $\text{GeNi}_{1.55}\text{Mg}_{0.45}\text{O}_4$ is illustrated in Fig. 2 and is normalized to the initial value measured at $t = 0$. A stretched exponential function with stretching coefficient $1-n$ was used to fit the M_{TRM} . In structural glass theory

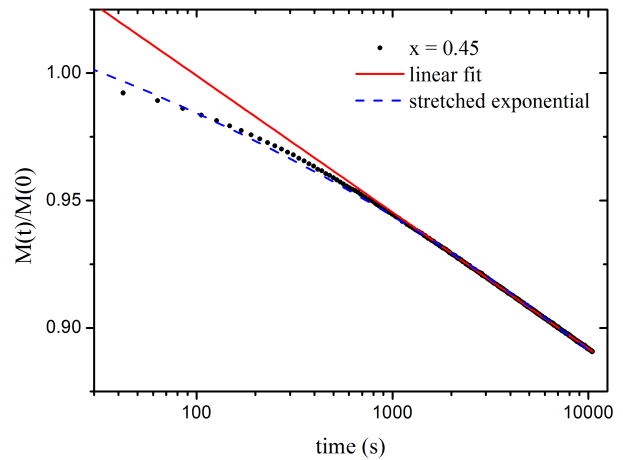


FIG. 2. [color online] M_{TRM} data for $\text{GeNi}_{1.55}\text{Mg}_{0.45}\text{O}_4$ taken over 10000 seconds after a wait time of 600 seconds. The dashed line is the resulting fit using a stretched exponential. The solid line is a linear fit that is constrained to the linear portion of the data.

it is known as the Kohlrausch-Williams-Watts (KWW) law and it is used to describe relaxation in physical properties of super-cooled liquids.^{29,30} In the context of magnetic glasses, this expression has been applied above and below T_g ³¹ with a temperature dependence of n near T_g .³² For NGO spin glasses, the values obtained for n are equal within associated error and have a mean of $n=0.861$ with a standard deviation of 0.002. This value falls outside the boundaries predicted using mean field percolation in glassy systems.³³ Departure from this mean field prediction is not unusual, results from structural glass formers show that small values of the stretching parameter $1-n$ correspond to fragile glasses. Physically, n is a measure of broadness in the relaxation spectrum, which results in a deviation from Arrhenius behavior.³⁴

C. Heat Capacity

The specific heat was measured for diluted samples ($x=0$ to 0.30) in the temperature range of 2 K to 300 K. The total heat capacity can be decomposed into the sum of lattice, magnetic and electronic contributions. In NGO, the electronic contribution is negligible and can be ignored. To obtain the lattice contribution a common approach is to use the low temperature limit ($T < \theta_D/50$) of the Debye model.³⁵ In NGO, particularly in the diluted samples, the ordering phenomena requires the addition of magnetic correlations just above T_N and both gapped and ungapped spin wave contributions to the heat capacity.¹⁶ One would require an accurate description of the dilution response to these spin wave contributions to yield a meaningful lattice heat capacity. In light of this, an alternative method based on Padé approximants,³⁶ which was employed here, allows one to fit convenient

regions of the specific heat to obtain the lattice contribution. The total heat capacity can be expressed as:

$$C_p = C_{\text{mag}} + A * C_{\text{padé}} + B * C_{E1} + C * C_{E2} \quad (3)$$

where the last three terms model the lattice contribution and the sum of A, B and C is 7. The Padé approximant method is designed to reproduce the Debye function through all temperature ranges. It therefore utilizes the same Debye assumptions³⁵ (harmonic approximation and isotropic spin waves) and represents only the acoustic modes. To account for the optical modes, two Einstein terms C_{E1} and C_{E2} , have been added, which take the form of equation 4. T_E is the corresponding Einstein temperature and R is the gas constant.

$$C_E = 3R \left(\frac{T_E}{T} \right)^2 \frac{e^{T_E/T}}{(e^{T_E/T} - 1)^2} \quad (4)$$

Figure 3 illustrates experimental data for $\text{Ni}_{1.99}\text{Mg}_{0.01}\text{GeO}_4$ and the resulting fit using the last three terms of equation 3. The temperature range for the fit is 100 K to 300 K, which was selected to be sufficiently far away from the magnetic transitions such that they have a negligible contribution to the specific heat.

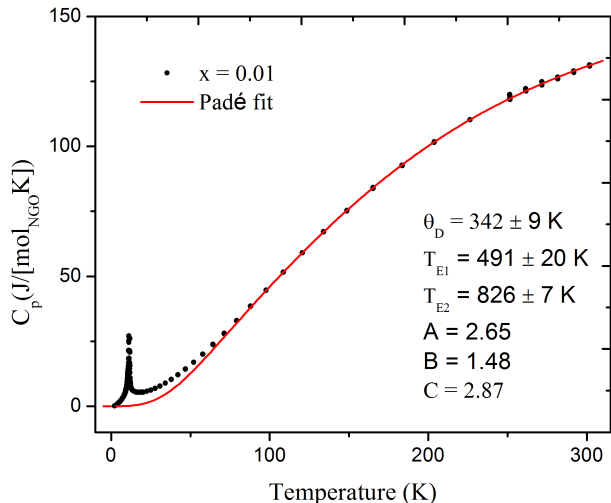


FIG. 3. [color online] Specific heat of $\text{Ni}_{1.99}\text{Mg}_{0.01}\text{GeO}_4$. The data is fitted from 120 K to 300 K to the last three terms of equation 3 with the fit line extrapolated to 0 K.

The Debye temperature obtained is $\Theta_D = 342 \pm 9$ K, which is smaller than the value of 386 K found by Lashley *et al.*¹⁶ Possible reasons for this difference could be their usage of the low temperature Debye form to temperatures as high as 75 K. Due to the approximations made in the Debye model, the value of Θ_D varies with temperature. This variation is minimized³⁵ in the temperature regions $T < \theta_D/50$ (7.72 K) and $T > \theta_D/2$ (193 K) if the 386 K value is assumed.

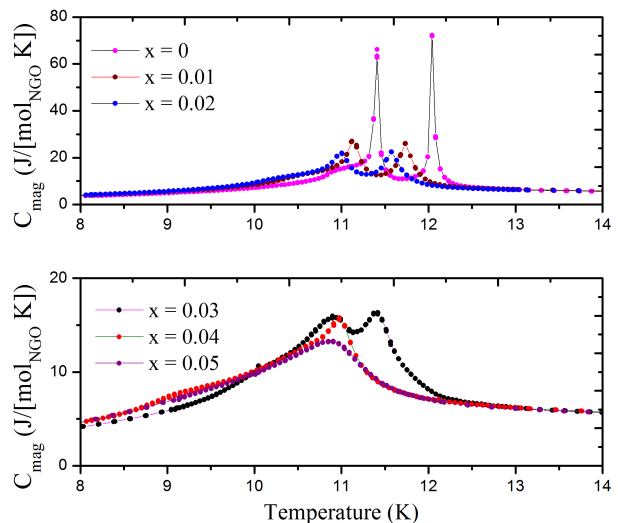


FIG. 4. [color online] Plot of the magnetic contribution to specific heat for several diluted samples of $\text{GeNi}_{2-x}\text{Mg}_x\text{O}_4$.

With the lattice contribution determined, the magnetic contribution can be calculated and is illustrated in Fig. 4. There is a reduction and broadening of the peaks in the specific heat, with increasing dilution of the the Ni^{2+} ions, which is evidence for a shift from long to short range ordering. We observe the disappearance of T_{N2} at 2.0% ($x = 0.04$) dilution while T_{N1} persists in a visible but broadened form. This indicates the destruction of long range order upon random site dilution occurs first in the triangular planes followed by the kagomé planes. This is interesting since one would expect dilution to affect kagomé ordering to a greater degree as there are three times the number of kagomé sites compared to triangular sites. A Mg^{2+} ion is three times more likely to sit on these planes, if the dilution is completely random amongst B sites. This result suggests a heightened importance of the linkage role that the kagomé sites, which are sandwiched between to triangular planes, provide to the network of triangular planes.

D. AC Susceptibility

With the destruction of long range order, the dynamic susceptibility becomes an important probe for determining the nature of the low temperature state. AC susceptibility measurements were completed on samples in the dilution range of $x = 0.15$ to 1.00 at 500, 1000, 5000 and 7000 Hz. Data for these dilution values, taken at 7000 Hz, is shown in Fig. 5. The onset of canonical spin glass behavior can be seen in dilution levels at, and above, 15%. In canonical spin glasses the freezing temperature T_f can be defined as the cusp in the real part of the AC susceptibility χ' and a spike in the imaginary part of the susceptibility χ'' . This behavior is due to the inability of spins to keep up with the oscillating applied

field, which diminishes the in phase component χ' , and causes a non-zero out of phase component χ'' .

In diluted NGO, there is a decrease in freezing temperature T_f with increased Mg^{2+} concentration, which follows a nearly linear response in the spin glass regime ($0.15 < x < 1.00$). Linear extrapolation of the data yields a non physical result of approximately $x = 3$ for the intercept on the temperature axis.

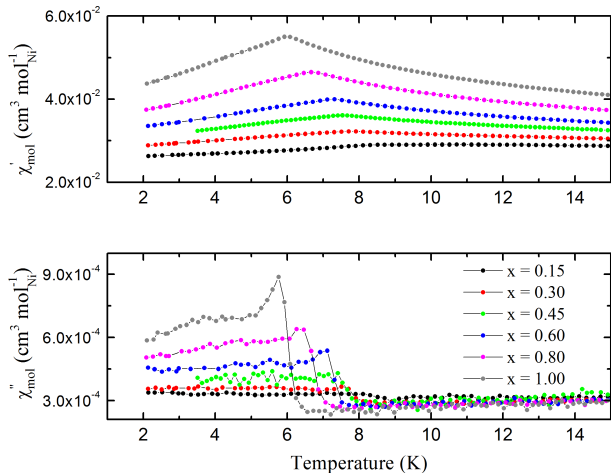


FIG. 5. [color online] Plot of the AC susceptibility of diluted samples taken at 7000 Hz. The cusp in the real part and jump in the imaginary part of the dynamic susceptibility indicate spin glass transitions.

An observed frequency dependence on T_f exists and is a characteristic feature of spin glasses and systems with broad distributions of energy levels.^{7,37} One way to compare this frequency dependence between different systems is to calculate δ , which is a measure of the drift of T_f with frequency. This is often defined as:

$$\delta = \frac{\Delta T_f}{T_f \Delta \ln(w)} \quad (5)$$

where $w = 2\pi f$ and f is the AC driving frequency. The value of δ can be used to determine the relative strength of interaction between the spin entities (clusters or single spins) of the spin glass.^{37,38} For weakly interacting systems, such as $\text{La}_{0.994}\text{Gd}_{0.006}\text{Al}_2$,³⁹ δ takes a value of 0.056. Conversely, for systems with stronger interactions such as canonical spin glasses, δ has an approximate value of 0.002³⁸. In $\text{Ni}_{2-x}\text{Mg}_x\text{GeO}_4$, δ takes values: 0.0061, 0.0074, 0.0065, 0.0084, 0.0091 for dilution levels of $x = 0.30, 0.45, 0.60, 0.80, 1.00$ respectively.

The frequency dependence of the spin glass freezing temperature can also be modelled using Arrhenius type, Vogel-Fulcher-Tamman law, power law, and stretched exponential.⁴⁰ In the Arrhenius model (τ is the inverse of AC driving frequency):

$$\tau = \tau_0 e^{\frac{E_a}{k_b T_f}} \quad (6)$$

one often finds that equation 6 yields non-physical results for the characteristic relaxation time τ_0 and activation energy E_a .³⁸ This deviation from Arrhenius behavior is a characteristic of a fragile glass former. A modification of the Arrhenius form yields the Vogel-Fulcher-Tamman (VFT) law, which was developed in structural glass literature to describe the temperature dependence of viscosity.⁴¹ It can be applied in systems with a broad distributions of relaxation times.

$$\tau = \tau_0 e^{\frac{E_a}{k_b(T_f - T_0)}} \quad (7)$$

Here T_0 is a measure of interaction strength between spin entities (clusters or single spins) and E_a is the activation energy. This form, although useful, creates ambiguity as T_0 is assigned in an ad-hoc manner to obtain what is believed to be physically relevant values for τ_0 .⁴⁰ To remedy this issue, one can utilize a power law form reminiscent of expressions used in other critical phenomena:

$$\tau = \tau_* \left(\frac{T_f - T_g}{T_g} \right)^{-zv} \quad (8)$$

where T_f , τ_* , T_g are the frequency dependent freezing temperature, the characteristic relaxation time and the freezing temperature as $f \rightarrow 0$. Rather than fitting all three parameters simultaneously, T_f was determined by the peak in the DC susceptibility. Observed data and the resulting fits to equations 7 and 8 are shown in Fig. 6 with values for the fitted parameters found in Table II.

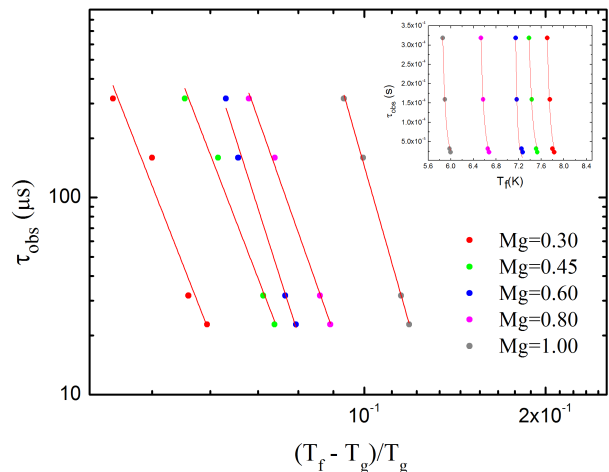


FIG. 6. [color online] Plot of AC freezing temperature data fitted to equation 8. Inset graph illustrates the same data fitted using the VFT equation.

The characteristic relaxation time of the spin glass system τ_* ranges from 10^{-14} to 10^{-16} seconds, which indicative of canonical spin glass behaviour. Contrast this with the so-called cluster glass systems like $\text{La}_{1.85}\text{Sr}_{0.15}\text{Cu}_{1-y}\text{Ni}_y\text{O}_4$, $\text{Li}_x\text{Ni}_{2-x}\text{O}_2$ and

TABLE II. Summary of AC susceptibility fit data on diluted samples.

Dilution (%)	zv	$\tau_*(10^{-15} s)$	$E_a(eV)$	$T_0(K)$
15	7.8 ± 1.0	3.2 ± 0.3	2.8 ± 0.2	6.44 ± 0.09
22.5	7.92 ± 0.6	19 ± 3	2.7 ± 0.2	6.03 ± 0.08
30	9.6 ± 0.6	0.50 ± 0.02	1.88 ± 0.06	6.34 ± 0.03
40	8.7 ± 0.3	17 ± 0.9	2.6 ± 0.1	5.28 ± 0.04
50	10.7 ± 0.3	2.8 ± 0.07	2.8 ± 0.1	4.56 ± 0.03

$\text{CaBaFe}_{4-x}\text{Li}_x\text{O}_7$, which have τ_* values of $10^{-9.5}$, 7.5×10^{-11} and 4.9×10^{-12} seconds respectively.^{37,42,43} The values of the critical exponent pair zv obtained vary from 7.8 to 10.7 and fall within the range 5 to 11 found for several spin glass compounds.⁴⁰

E. High Pressure Effects

Lattice distortion is an important process that can relieve frustration. This is evident particularly in the related spinel GeCo_2O_4 , which undergoes a simultaneous cubic to tetragonal distortion and antiferromagnetic transition, where $c/a \approx 1.0014$.⁴⁴ To the authors' knowledge, there has been no evidence of a structural transition in NGO using neutron or synchrotron x ray probes.¹⁸ The relation between lattice constant and the corresponding magnetic properties of NGO can be further tested using high precision thermal expansion measurements. The results are illustrated in Fig. 7 where the reference length L_0 is $L(T = 20)$. The two AFM transitions are clearly indicated by a steep decrease in strain $\Delta L/L_0$ indicating lattice constant shrinkage. This decrease is affected by applied magnetic field and is most noticeable at the kagomé ordering temperature T_{N1} . Specifically, the change in strain during ordering at T_{N1} is -6.899×10^{-6} , -4.943×10^{-6} , and 1.082×10^{-6} for fields of 0, 1.5, and 6.0 T respectively. A similar field induced transition in the nature of TE response has been observed⁴⁵ in EuTiO_3 where a cross over between contraction and expansion occurred at 0.675 T, with destruction of long range order at 1 T. Conversely, NGO is very robust against applied fields with a spin flop transitions at $H_1 = 30$ T and $H_2 = 37$ T at 4 K.⁴⁶

This result suggests that a spin-lattice coupling occurs in NGO. To further test the effects of perturbations on Ni_2GeO_4 , quasi-hydrostatic high pressure susceptibility measurements were taken on a polycrystalline sample in the range 0 to 1.2 GPa. To estimate the effect of applied pressure on the lattice it is noted⁴⁷ that several related spinel compounds have bulk moduli K that lie in between 170 to 210 GPa. Using a value of 200 GPa the strain can be estimated using $K = -V\Delta P/\Delta V$ where $\Delta V \approx 3L^2\Delta L$ the maximum strain is 10^{-3} .

Figure 8 illustrates the effect of applied quasi-hydrostatic pressure on the two AFM transitions of poly-

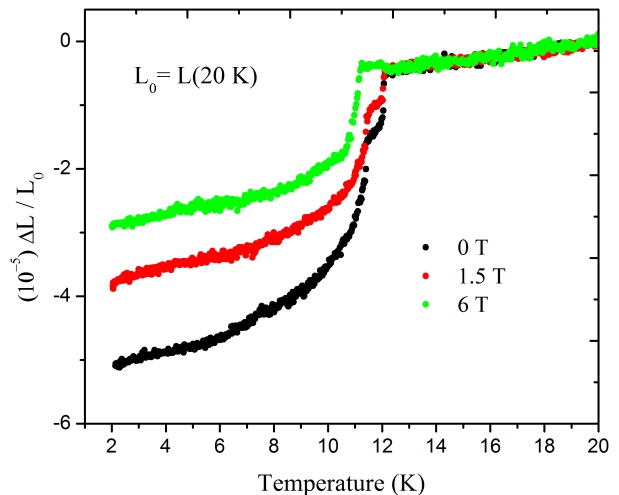


FIG. 7. [colour online] Strain $\Delta L/L_0$, taken at various applied fields, where L_0 is the reference length at 20 K. The onset of magnetic transitions are denoted by a rapid change in strain.

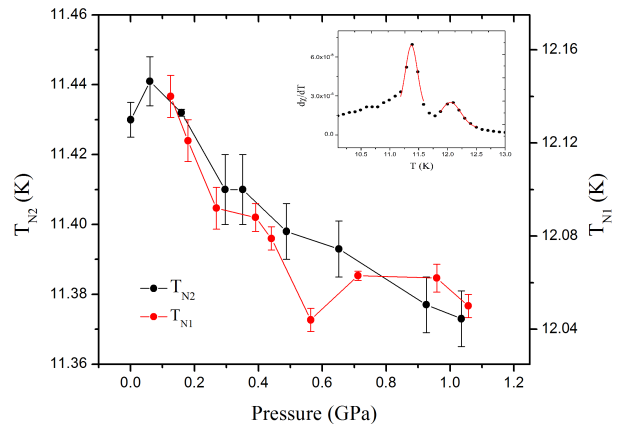


FIG. 8. [colour online] Antiferromagnetic transitions T_{N1} (kagomé) and T_{N2} (triangular) in GeNi_2O_4 at various applied pressures. The inset graph depicts fits to peaks in $d\chi/dT$.

crystalline NGO. These were determined by fitting Gaussian peak functions to maxima in $d\chi/dT$, which is shown in the inset. There is a small decrease of similar magnitude in the ordering temperatures T_{N1} and T_{N2} . The observation that both transitions have nearly identical responses is somewhat striking for several reasons. First, the kagomé and triangular planes order independently and, as seen in the strain data, yield vastly different lattice effects under applied fields. Furthermore, the exchange connectivity for each plane type is different with the kagomé planes having more nearest-neighbors that reside in the same plane. These results depict a magnetically robust system that can withstand lattice changes of varying degree, but still maintain the necessary balance in exchange interactions that yield two AFM transitions.

IV. DISCUSSION

Combining the results from specific heat, AC and DC susceptibility measurements, one can construct a phase diagram which is shown in Fig. 9. There are 3 distinct magnetic phases separated by an indeterminate region, which has no distinct features of a spin glass transition or long range ordering.

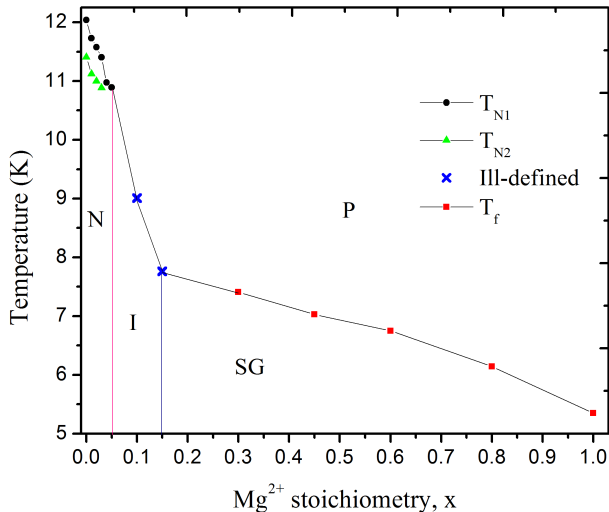


FIG. 9. [colour online] Experimental phase diagram of magnetically diluted $\text{GeNi}_{2x}\text{Mg}_x\text{O}_4$. There are 4 distinct regions: N - Néel ordered, I - ill defined, SG - spin glass, and P - paramagnetic.

A. Low Dilution $x < 0.10$

The effects of B site magnetic dilution appear have a dramatic effect on the two long range ordered, low temperature states. The magnitude of this effect varies for the different planar types that make up the B site sub-lattice. Figure 9 illustrates that long range order persists in the kagomé and triangular planes up to dilution values up to $x=0.05$ and $x=0.03$ respectively. In this region the Néel temperatures associated with T_{N1} and T_{N2} evolve linearly and can be extracted to yield the critical dilution level of $x_{d1} = 0.53 \pm 0.07$ and $x_{d2} = 0.70 \pm 0.1$. This corresponds to a critical concentration of $p_{c1} = 0.74 \pm 0.04$ for the kagomé planes and $p_{c2} = 0.65 \pm 0.05$ for the triangular planes. The expected 2 dimensional values for these planar types with nearest-neighbor interactions are 0.652 (kagomé) and 0.5 (triangular). This is an unusual result as one would expect the experimental values of p_c to be smaller than the 2D values. NGO is the antithesis of a 2D system with large interplanar coupling, which is believed to give rise to NGO's unique ground state.¹⁹ Increases in dimensionality should reduce p_c as the lattice becomes more connected. For example, the percolation threshold for stacked kagomé and triangular lattices have values⁴⁸

of 0.3345 and 0.2623 respectively, much lower than 2D analogues. Similarly, if interactions extend beyond nearest neighbours, the ordered state becomes very robust with respect to magnetic site removal.⁴⁹

However, seemingly artificial levels for critical concentration are not unheard of. In the kagomé staircase $(\text{Co}_{1-x}\text{Mg}_x)_3\text{V}_2\text{O}_8$, it was found to have an $x_c = 0.74$ instead of 0.65 for Néel ordering. This was determined to stem from the buckled nature of the kagomé staircase structure, that quenches exchange interactions from the spine sites, which increases p_c from the expected 0.65 to 0.74.⁵⁰ In NGO, there is no evidence of major structural distortion,¹⁸ such as buckling, that would result in the loss of interactions. Furthermore, NGO is a highly 3D system with large spin connectivity due to its large exchange network.

One possibility for this high sensitivity to dilution is the effect of coupling between the spins that reside on different plane types. That is, due to the distinct ordering of the kagomé and triangular planes below T_{N2} , one can think of the B site lattice as two, 3D interconnected networks: stacked triangular and stacked kagomé. These networks have connections to themselves and to each other. Factoring up to J_4 with 42 total neighbours, a single spin in the triangular network contains 12 links to other triangular sites and 30 links to the kagomé network. Conversely, the kagomé system is much more self connected with only 10 links to the triangular network and 30 to other kagomé sites. Recent research⁵¹ has shown that coupled networks, a network of networks (NON), are more vulnerable to what is often called 'attack', which in this context is site dilution. This vulnerability is manifested as an increased percolation threshold⁵² and has been observed in several different network types: Erdos-Renyi, regular random, and lattice.⁵³ Furthermore, with increased internetwork coupling, the more vulnerable the NON becomes, which results in larger p_c thresholds. This is in stark contrast to single networks where increased connectivity tends to decrease p_c .^{48,52,54} Physically, this can be understood as a diluted site, on either kagomé or triangular layers, affecting both its own layer type as well as the other complementary layer. This perturbation could cascade locally through both networks amplifying its effect.

B. Spin Glass ($0.30 \leq x \leq 1.0$)

A broad specific heat anomaly and a jump in the imaginary component of the AC susceptibility results indicate a single spin glass transition that begins at $x = 0.30$ (15% dilution). Somewhat surprisingly, glassiness does not form on each plane type, which would presumably give rise to two distinct freezing transitions: one for kagomé and one for triangular spins. Instead there is a single spin glass transition. It is unclear if the glass state emerges across the entire B site sub-lattice, or only on the kagomé sites while the triangular planes behave in

paramagnetic fashion. Specific heat results suggest the latter case due to the apparent destruction of the T_{N2} in Fig. 4, rather than the broadening and merger of both peaks. If the glass state is only composed of kagomé sites, one can compare the above results with structurally similar systems that undergo spin glass transitions.

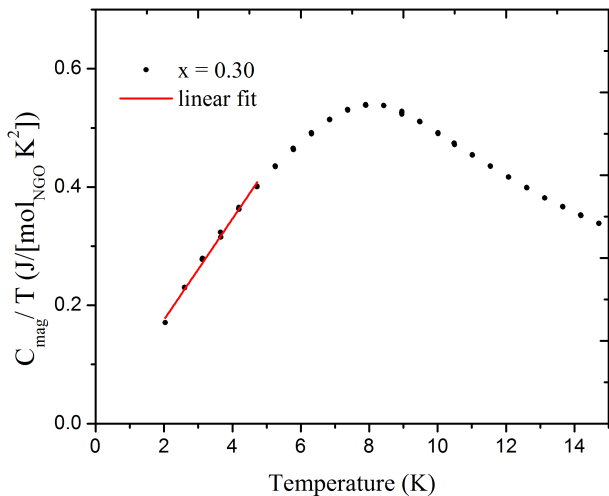


FIG. 10. [colour online] Magnetic component of C_p/T for the spin glass $\text{GeNi}_{1.7}\text{Mg}_{0.3}\text{O}_4$. The red linear fit line indicates a T^2 dependence of the magnetic specific heat at low temperature.

One such system, deuteronium jarosite ($\text{D}_3\text{O})\text{Fe}_3(\text{SO}_4)_2(\text{OD})_6$, consists of Fe^{3+} ions ($S=5/2$) in stacked kagomé planes, which undergoes a spin glass transition at 13.8 K.⁵⁵ Specific heat results indicate an anomalous low temperature T^2 behaviour, instead of the linear relationship expected for canonical spin glasses. Similar behaviour has been found in $\text{SCGO}(x)$ spin glasses.⁵⁶ In both cases, it is believed that the T^2 dependence stems from the strong 2D character of the kagomé planes,⁵⁷ which are the magnetic building blocks of the compounds. In the spin glass $\text{GeNi}_{1.7}\text{Mg}_{0.3}\text{O}_4$ there is a low temperature T^2 dependence, illustrated in Fig. 10, which could indicate a similar 2D character. Furthermore, the δ value for diluted NGO range from 0.006 to 0.009 compare favourably to deuteronium jarosite where $\delta = 0.01$. In addition, these numbers are comparable the values obtained for canonical spin glasses such as CuMn ($\delta = 0.002$),⁵⁸ and AuMn ($\delta=0.0020$).⁵⁹

V. CONCLUSIONS

In this paper the effects of magnetic dilution and spin-lattice coupling on spinel type GeNi_2O_4 are reported. This was undertaken to probe the nature of the long range ordered state of NGO that is formed by two closely spaced magnetic transitions, the root of which, is a complex exchange network of 32 relevant neighbours. Thermal expansion measurements reveal a field dependent lattice contraction at both T_{N1} and T_{N2} . At an applied magnetic field of 6 T, there is a positive change in strain indicating a field induced cross over from lattice contraction to expansion. The phase evolution of this compound when Ni^{2+} sites are replaced with non-magnetic Mg^{2+} can be broadly classified into three regions: ordered, ill defined, and spin glass.

At dilution levels of $x = 0.30$ and higher the system becomes a spin glass. AC susceptibility and thermoremanent magnetization measurements suggest that the system is a canonical type glass. In addition, there is no evidence of distinct spin glass transitions for each of the AFM transitions observed in the parent compound. It appears that the triangular planes first become disordered, followed by a glass transition in the kagomé planes. The magnetic specific heat in the glassy state has a T^2 character at low temperature, which is unusual for spin glass compounds. This suggests a shift from 3D long range ordered state to a 2D spin glass.

Lastly, the long range ordered state of the kagomé and triangular planes are extremely susceptible to magnetic dilution. Specific heat and magnetic susceptibility measurements indicate that clear signs of magnetic ordering disappear for kagomé spins at approximately 2.5% Mg^{2+} substitution. Likewise, the ordered state for triangular spins appear even more delicate, with a lack of distinct ordering at 1.5% dilution. Through linear fits the percolation thresholds for the kagomé and triangular planar networks were found to be $p_{c1} = 0.74 \pm 0.04$ and $p_{c2} = 0.65 \pm 0.05$ respectively. These values are much larger than percolation values for stacked kagomé ($p_c = 0.3346$) and triangular planes ($p_c = 0.2623$). This perplexing result can possibly be explained by treating the triangular and kagomé spins as a network of networks. NONs have been shown to be highly unstable to site removal which is amplified by increased connectivity.⁵² Neutron diffraction experiments currently undertaken will hopefully shed light on the nature of the ill-defined phase and the anomalously large percolation threshold. If the NON interpretation is correct, to the author's knowledge, NGO could be the first reported manifestation of this effect in the solid state. Further research in other magnetic systems with distinctly ordered sublattices, such as $\text{Gd}_2\text{Ti}_2\text{O}_7$,⁶⁰ could be studied to find other candidates.

* Jory Korobanik jory.korobanik@brocku.ca

¹ C. R. Wiebe and A. M. Hallas,

- APL Materials **3**, 041519 (2015).
- ² L. Balents, Nature **464**, 199 (2010).
 - ³ S. Ji, S.-H. Lee, C. Broholm, T. Y. Koo, W. Ratcliff, S.-W. Cheong, and P. Zschack, Phys. Rev. Lett. **103**, 037201 (2009).
 - ⁴ C. Castelnovo, R. Moessner, and S. L. Sondhi, Nature **451**, 42 (2008).
 - ⁵ K. Fischer and J. Hertz, *Spin Glasses*, Cambridge Studies in Magnetism (Cambridge University Press, 1993).
 - ⁶ M. J. Harris, S. T. Bramwell, D. F. McMorrow, T. Zeiske, and K. W. Godfrey, Phys. Rev. Lett. **79**, 2554 (1997).
 - ⁷ K. Binder and A. P. Young, Rev. Mod. Phys. **58**, 801 (1986).
 - ⁸ H. Diep, *Frustrated Spin Systems* (World Scientific, 2013).
 - ⁹ S. H. Kang, S. Shan, A. Košmrlj, W. L. Noorduin, S. Shian, J. C. Weaver, D. R. Clarke, and K. Bertoldi, Phys. Rev. Lett. **112**, 098701 (2014).
 - ¹⁰ A. P. Ramirez, Annual Review of Materials Science **24**, 453 (1994).
 - ¹¹ J. E. Greedan, J. Mater. Chem. **11**, 37 (2001).
 - ¹² J. S. Gardner, M. J. P. Gingras, and J. E. Greedan, Rev. Mod. Phys. **82**, 53 (2010).
 - ¹³ A. Navrotsky and L. Hughes, Journal of Solid State Chemistry **16**, 185 (1976).
 - ¹⁴ C. Lacroix, P. Mendels, and F. Mila, *Introduction to Frustrated Magnetism: Materials, Experiments, Theory*, Springer Series in Solid-State Sciences (Springer, 2011).
 - ¹⁵ S.-H. Lee, C. Broholm, W. Ratcliff, G. Gasparovic, Q. Huang, T. H. Kim, and S.-W. Cheong, Nature **418**, 856 (2002).
 - ¹⁶ J. Lashley, R. Stevens, M. Crawford, J. Boerio-Goates, B. Woodfield, Y. Qiu, J. Lynn, P. Goddard, and R. Fisher, Physical Review B **78**, 104406 (2008).
 - ¹⁷ T. Yamada, Z. Hiroi, M. Takano, M. Nohara, and H. Takagi, Journal of the Physical Society of Japan **69**, 1477 (2000).
 - ¹⁸ M. Crawford, R. Harlow, P. Lee, Y. Zhang, J. Hormadaly, R. Flippen, Q. Huang, J. Lynn, R. Stevens, B. Woodfield, J. Boerio-Goates, and R. Fisher, Physical Review B **68**, 220408 (2003).
 - ¹⁹ M. Matsuda, J. H. Chung, S. Park, T. J. Sato, K. Matsuno, H. A. Katori, H. Takagi, K. Kakurai, K. Kamazawa, Y. Tsunoda, I. Kagomiya, C. L. Henley, and S. H. Lee, EPL (Europhysics Letters) **82**, 37006 (2008).
 - ²⁰ N. Ashcroft and N. Mermin, *Solid State Physics*, HRW international editions (Holt, Rinehart and Winston, 1976).
 - ²¹ S.-H. Lee, W. Ratcliff, Q. Huang, T. Kim, and S.-W. Cheong, Physical Review B **77**, 014405 (2008).
 - ²² D. Fiorani, S. Viticoli, J. L. Dormann, J. L. Tholence, and A. P. Murani, Phys. Rev. B **30**, 2776 (1984).
 - ²³ A. Eiling and J. S. Schilling, Journal of Physics F: Metal Physics **11**, 623 (1981).
 - ²⁴ R. D. Shannon, Acta Crystallographica Section A **32**, 751 (1976).
 - ²⁵ A. R. Denton and N. W. Ashcroft, Phys. Rev. A **43**, 3161 (1991).
 - ²⁶ S. Diaz, S. de Brion, G. Chouteau, B. Canals, V. Simonet, and P. Strobel, Physical Review B **74**, 092404 (2006).
 - ²⁷ R. L. Carlin, *Magnetochemistry* (Springer-Verlag, 1986).
 - ²⁸ B. Martínez, F. Sandiumenge, A. Rouco, A. Labarta, J. Rodríguez-Carvajal, M. Tovar, M. Causa, S. Galí, and X. Obradors, Phys. Rev. B **46**, 10786 (1992).
 - ²⁹ G. Williams and D. C. Watts, Trans. Faraday Soc. **66**, 80 (1970).
 - ³⁰ M. Klinger, *Glassy Disordered Systems: Glass Formation and Universal Slow Dynamics at Low Temperatures* (World Scientific, 2013).
 - ³¹ M. A. Continentino and A. P. Malozemoff, Phys. Rev. B **33**, 3591 (1986), mTRM.
 - ³² R. V. Chamberlin, G. Mozurkewich, and R. Orbach, Phys. Rev. Lett. **52**, 867 (1984).
 - ³³ G. Lois, J. Blawdziewicz, and C. S. O'Hern, Phys. Rev. Lett. **102**, 015702 (2009).
 - ³⁴ K. L. Ngai, A. K. Rajagopal, and C. Y. Huang, Journal of Applied Physics **55**, 1714 (1984).
 - ³⁵ E. Gopal, *Specific Heats at Low Temperatures*, International cryogenics monograph series (Plenum Press, 1966).
 - ³⁶ R. J. Goetsch, V. K. Anand, A. Pandey, and D. C. Johnston, Phys. Rev. B **85**, 054517 (2012).
 - ³⁷ A. Malinowski, V. L. Bezusyy, R. Minikayev, P. Dziawa, Y. Syryanny, and M. Sawicki, Phys. Rev. B **84**, 024409 (2011).
 - ³⁸ J. L. Dormann, L. Bessais, and D. Fiorani, Journal of Physics C: Solid State Physics **21**, 2015 (1988).
 - ³⁹ J.-L. Tholence, Physica B+C **126**, 157 (1984).
 - ⁴⁰ J. Souletie and J. L. Tholence, Phys. Rev. B **32**, 516 (1985).
 - ⁴¹ S. Shtrikman and E. Wohlfarth, Physics Letters A **85**, 467 (1981).
 - ⁴² K. Vijayanandhini, C. Simon, V. Pralong, V. Caignaert, and B. Raveau, Phys. Rev. B **79**, 224407 (2009).
 - ⁴³ S. A. Kumar, Journal of Physics: Condensed Matter **25**, 496001 (2013).
 - ⁴⁴ T. Hoshi, H. A. Katori, M. Kosaka, and H. Takagi, Journal of Magnetism and Magnetic Materials **310**, e448 (2007), proceedings of the 17th International Conference on Magnetism The International Conference on Magnetism.
 - ⁴⁵ P. G. Reuvekamp, R. K. Kremer, J. Köhler, and A. Bussmann-Holder, Phys. Rev. B **90**, 094420 (2014).
 - ⁴⁶ S. Diaz, S. de Brion, M. Holzappel, G. Chouteau, and P. Strobel, Physica B: Condensed Matter **346-347**, 146 (2004).
 - ⁴⁷ A. M. Hofmeister, Journal of Geophysical Research: Solid Earth **96**, 16001 (1991).
 - ⁴⁸ S. C. van der Marck, Phys. Rev. E **55**, 1514 (1997).
 - ⁴⁹ D. Fiorani, L. Gastaldi, A. Lapiccirella, S. Viticoli, and N. Tomassini, Solid State Communications **32**, 831 (1979).
 - ⁵⁰ K. Fritsch, Z. Yamani, S. Chang, Y. Qiu, J. R. D. Copley, M. Ramazanoglu, H. A. Dabkowska, and B. D. Gaulin, Phys. Rev. B **86**, 174421 (2012).
 - ⁵¹ S. Havlin, D. Kenett, A. Bashan, J. Gao, and H. Stanley, The European Physical Journal Special Topics **223**, 2087 (2014).
 - ⁵² S. V. Buldyrev, R. Parshani, G. Paul, H. E. Stanley, and S. Havlin, Nature **464**, 1025 (2010).
 - ⁵³ A. Bashan, Y. Berezin, S. V. Buldyrev, and S. Havlin, Nature Physics **9**, 667 (2013).
 - ⁵⁴ D. Stauffer and A. Aharony, *Introduction To Percolation Theory* (Taylor & Francis, 1994).
 - ⁵⁵ A. S. Wills, A. Harrison, S. A. M. Mentink, T. E. Mason, and Z. Tun, EPL (Europhysics Letters) **42**, 325 (1998).
 - ⁵⁶ A. P. Ramirez, G. P. Espinosa, and A. S. Cooper, Phys. Rev. Lett. **64**, 2070 (1990).
 - ⁵⁷ A. P. Ramirez, G. P. Espinosa, and A. S. Cooper, Phys. Rev. B **45**, 2505 (1992).
 - ⁵⁸ C. A. M. Mulder, A. J. van Duyneveldt, and J. A. Mydosh, Phys. Rev. B **25**, 515 (1982).
 - ⁵⁹ C. A. M. Mulder, A. J. van Duyneveldt, and J. A. Mydosh, Phys. Rev. B **23**, 1384 (1981).
 - ⁶⁰ R. A. Stone, *Universal Low-Energy Properties of Disordered Systems* (World Scientific, 2013).

